

Estimation of dispersion in orientations of natural fractures from seismic data: Application to DFN modeling and flow simulation

REINALDO J. MICHELENA, KEVIN S. GODBEY, HUABING WANG, and JAMES R. GILMAN, *iReservoir.com*
CHRIS K. ZAHM, *University of Texas at Austin*

This article describes a statistical methodology to estimate dominant fracture orientation and dispersion from seismically calculated 3D structural attributes. The orientation-dispersion parameter is a modified version of the circular variance that is independent of direction and can be used to compute the Fisher coefficient, a key parameter in the probability density function used in discrete-fracture-network (DFN) modeling to stochastically generate fracture orientations. We show examples of applications to seismic-constrained DFN modeling and perform flow simulations on fractured models built using different dispersion-parameter models to discuss possible implications for drainage of naturally fractured unconventional reservoirs.

Introduction

The design of horizontal wells and hydraulic-fracture stimulation requires a detailed understanding of the variations in relative orientations of natural fractures and the local stress field across the reservoir. Existing natural fractures strongly influence the effectiveness of any stimulation program. Structural attributes extracted from poststack 3D seismic data such as curvature, semblance, or dip have been used in the estimation of preferential orientation in the subsurface, particularly orientation of natural fractures. Attributes derived from the analysis of prestack amplitude variations versus offset and azimuth (AVOZ) have also been used for this purpose. After careful calibration with log-derived fracture orientations, orientations derived from seismic data may be used as a proxy for orientations of natural fractures. However, these orientations can be misleading or difficult to interpret when multiple fracture orientations are present.

The model-based nature of AVOZ analyses (which assume either a single set of vertical fractures, two sets of orthogonal vertical fractures, or either of the above with a tilted axis of symmetry) may yield uncertain results when the assumptions of the fracture model are not met. In many geologic settings, several nonorthogonal fracture sets occur with different dips and azimuths that overlap in the same volume of rock. Approaches that use poststack data and overcome the model-based limitations of using prestack data typically yield a single orientation per sample, with no indication of how to interpret it when multiple orientations are present.

Chopra et al. (2009), however, go beyond single-orientation answers. The authors generate what they refer to as “3D rose diagram” volumes after analyzing orientations of the azimuth of minimum curvature for each horizontal time slice. Even though their rose diagrams provide a visual idea of the dispersion in fracture orientation, no quantitative estimates of this dispersion are generated. Furthermore, rose diagrams

based on 2D time slices fall short in capturing the real 3D nature of fracture orientation that requires two parameters (dip and dip azimuth) instead of only the one used to generate rose diagrams (dip azimuth).

Natural fracture orientations and intensities derived from seismic data can be used to constrain discrete-fracture-network (DFN) modeling as long as careful calibration of the seismic attribute with local well data is performed to test whether the attribute carries information about actual natural fractures (e.g., Will et al., 2005). More information besides average orientation is required to construct a stochastically generated DFN model.

DFN modeling also requires a parameter called the Fisher coefficient that measures the dispersion in fracture orientations (Mardia, 1972). A high Fisher coefficient is related to fractures aligned primarily in one orientation, whereas a low value indicates fractures with many orientations. Even though the Fisher coefficient is three-dimensional in nature, it is usually estimated from 1D image-log data which record dip and dip azimuth only for fractures that intersect the well, hence suffering from sampling bias. The average orientation and degree of dispersion are estimated along the well and assumed to be constant in the interwell region in DFN modeling applications. Because of this assumption, local orientations

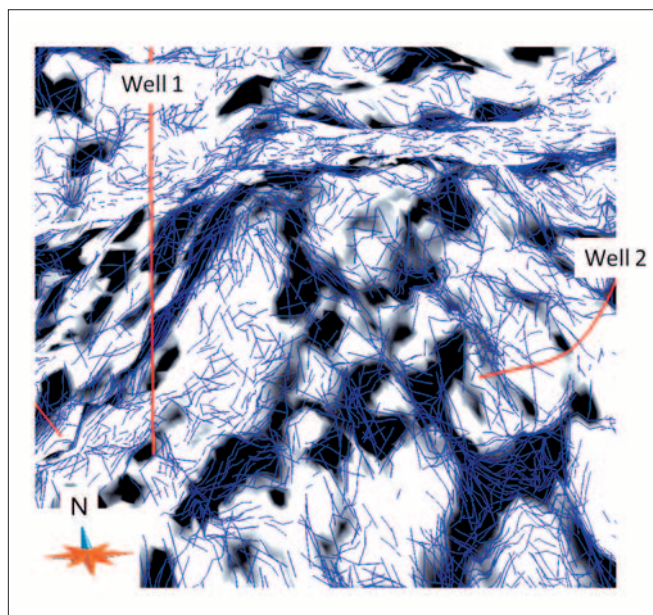


Figure 1. Local strike orientations (blue lines) overlaid on the maximum curvature attribute extracted along a stratigraphic horizon. Blue strike lines are centered in a 25- × 25-m cell-size surface. Only strikes related to the largest gradients are shown. The statistical analysis of these apparently “noisy” orientations may reveal important information about dispersion in fracture orientation in the reservoir.

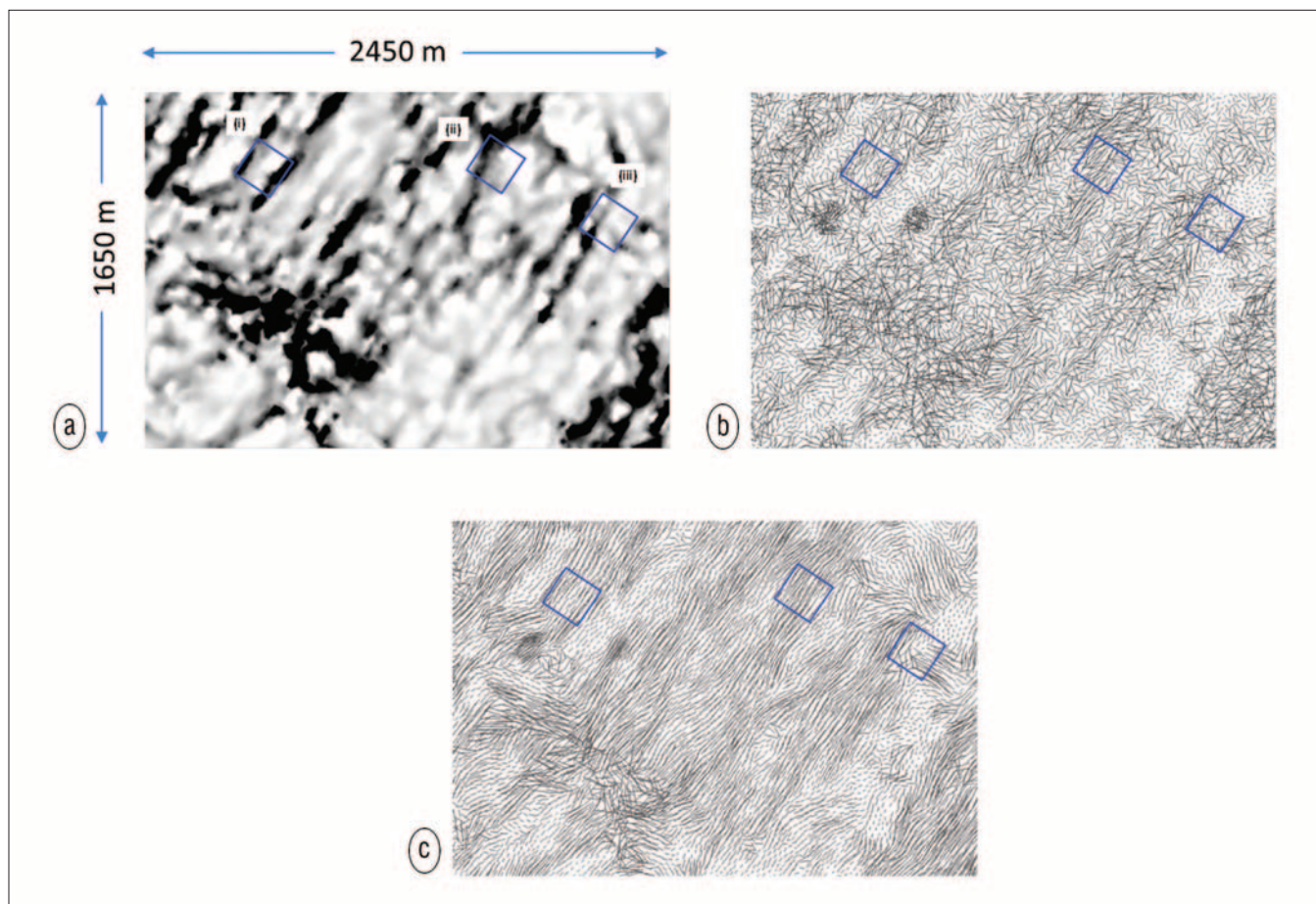


Figure 2. (a) Horizon slice of maximum curvature with areas of interest (in blue). (b) Original local fault strikes estimated by using the gradient of the maximum curvature. (c) Dominant orientations (mode) are extracted from moving blocks of $200\text{ m} \times 200\text{ m} \times 20\text{ m}$ and assigned to the center of each block. The length of the segments is proportional to the magnitudes of the local gradient. Areas indicated by blue squares will be analyzed in detail in Figure 3.

of modeled fractures will have the same dispersion as those at the wells, a hypothesis that might not necessarily be valid, implying that estimates of 3D variability in orientation dispersion from seismic data are needed.

We propose a methodology to estimate dominant orientations and orientation dispersion from structural seismic attributes that can be used to constrain DFN models. First, we start by extracting dip and dip-azimuth information from the chosen structural attribute and compare the results with orientations derived from image-log data. Because orientation may vary significantly within small areas, we extract a more consistent and less noisy dominant orientation and capture dispersion in the orientations by estimating a quantity that generalizes the concept of circular variance, is independent of the direction of the reference axis for angles,

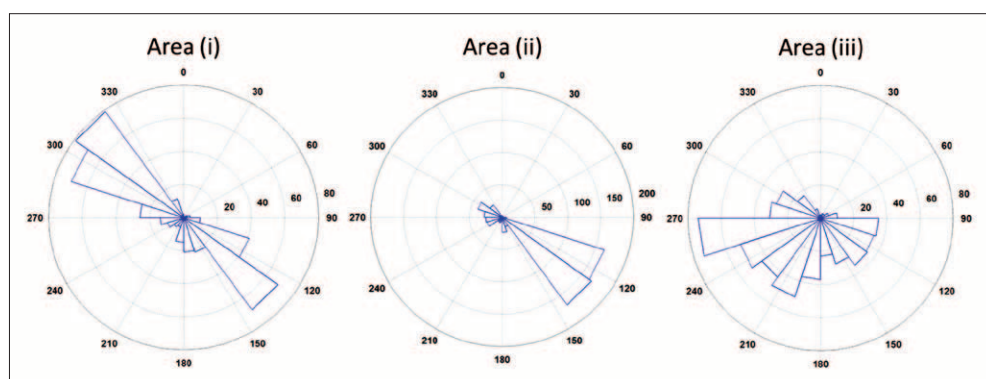


Figure 3. Dip-azimuth rose diagrams for the areas highlighted in Figure 2. Area (i) shows dips toward the northwest and southeast, and area (ii) shows dips predominantly southeast. Areas (i) and (ii) show that most dip azimuths are clustered around the same angles, whereas area (iii) shows more dispersion.

and can be transformed easily into the Fisher coefficient used for DFN modeling.

We elaborate on the meaning of this dispersion and explain how to estimate it from seismic data. Then we show how to use dominant orientation and dispersion volumes to constrain DFN modeling. The value of the approach is demonstrated with a simple DFN modeling example that

incorporates fracture intensity, dominant orientation, and orientation dispersion from seismic data into the modeled fractures. Finally, we build simple flow-simulation models using parameters typical of unconventional reservoirs to illustrate the importance of fracture dispersion in the drainage of unconventional reservoirs.

Orientations from structural attributes

Once the interpreter selects the attribute(s) that best respond to faulting and possible natural fractures by doing careful calibration with well data, we need to estimate orientations from this attribute(s) that can be related to local fault planes. We use the local 3D gradient of the attribute to achieve this goal. The calculation of the gradient in three dimensions also requires velocity information or a structural attribute volume in depth domain if meaningful estimates of the real dip are to be extracted, analyzed, and calibrated with well information. The plane perpendicular to the 3D gradient at each point in the volume can be interpreted as a local fault plane.

Figure 1 shows the intersection of local fault planes with a stratigraphic horizon which results in the blue segments parallel to local fault strikes. The attribute represented in this figure is the maximum curvature. Notice how variable local strikes can be within fault anomalies particularly. Even though these local orientations might look like “noise” in some areas, we will show that they contain valuable information about the possible dispersion in subseismic fracture orientations. The following section describes how to estimate this dispersion.

Statistics of seismic-derived orientations

As we discussed in the previous section, local fault orientations estimated from the 3D gradient might look noisy and even unreasonable in some areas. Because of a variety of reasons that range from data-quality issues and resolution to structural

complexity, local strikes estimated from the gradient are not necessarily reliable on a “point-by-point” basis. However, we propose that when analyzed collectively in a statistical manner,

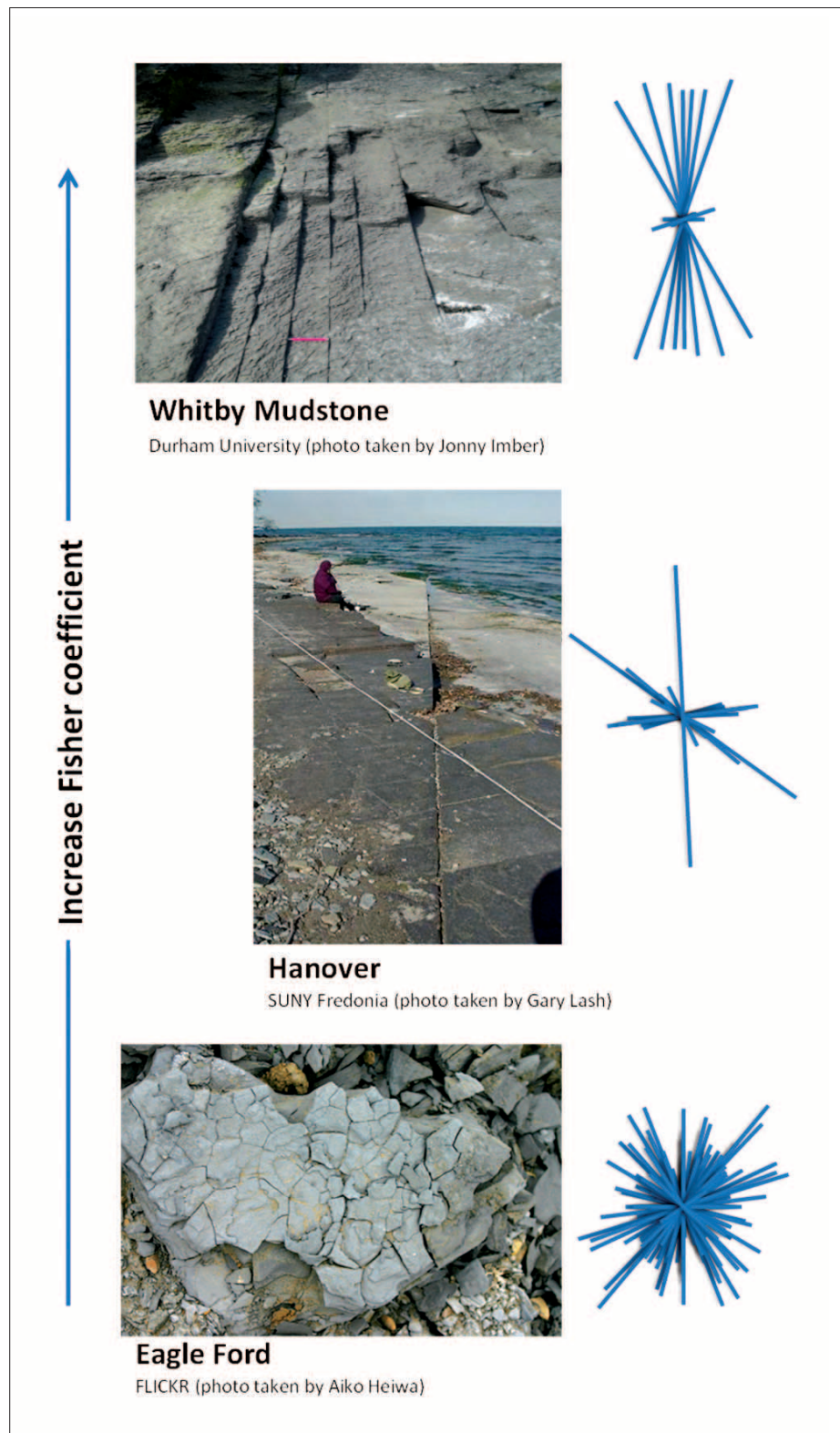


Figure 4. Plan views of shale outcrops showing significant variability in fracture dispersion for different formations. The qualitative fracture interpretations at the right indicate that the Fisher coefficient increases from Eagle Ford to Whitby mudstone, although changes within individual formations are also possible.

these “noisy” orientations might reveal important information about dispersion in subseismic fracture orientation across the reservoir. The calibration of these orientations with log-derived orientations should also be done in statistical terms.

Mean or dominant fracture orientation? To understand the variability in fracture orientation across the area of interest, we can extract different statistical measures from angles within small blocks of cells in the larger 3D volume, and these results are assigned back to the center of the block in a moving-average manner. For instance, we can compute local histograms of angles (rose diagrams), as proposed by Chopra et al. (2009), to analyze the variability in dip azimuth. We can also extract polar plots to analyze the real 3D nature of the fracture orientation that requires dip and dip-azimuth angles.

The simplest measure we can extract from a set of angles in a given subvolume is the average. This measure, however, can be misleading because circular variables such as angles cannot always be averaged as if they were linear variables. Even if we do the angle average properly by averaging the unit vectors that correspond to each orientation, the result can still be misleading because we might end up with average orientations that have nothing to do with the orientations observed in the field.

For instance, if two dominant fracture orientations at 0° and 90° , respectively, are observed in the reservoir, an average orientation of 45° is meaningless from the fluid-flow point of view. A measure that does not suffer from these limitations is the mode of the histogram, or dominant fault orientation. We think the mode is a more sensible estimate of an “equivalent” angle in a block where multiple orientations are present.

Figure 2a shows the maximum curvature extracted along a stratigraphic horizon, along with small segments indicating local strike orientations derived from the gradient and projected along the horizon (Figure 2b). Notice how the dominant angles (Figure 2c) are less noisy and more consistent across the area. Figure 3 shows rose diagrams for the areas highlighted in Figure 2. Areas (i) and (ii) show similar fracture strike orientation, with the difference that in area (ii), most fractures dip toward the southeast, whereas in area (i), fractures dip toward both northeast and southwest. Fractures in area (iii) are oriented in many directions. Most dips in the large area (not shown) are between 60° and 80° . Rose diagrams that correspond to areas (i), (ii), and (iii) are shown in Figure 3.

Dispersion in fracture orientation. Like in linear statistics, where a single number such as the mean or mode is insufficient to describe the shape or distribution of a set of numbers and higher moments such

as the variance are also needed, in circular statistics, we can also estimate a circular variance V as follows (Fisher, 1995):

$$V = 1 - R/N, \quad (1)$$

where N is the total number of angles used for the analysis and R is the magnitude of the vector sum of all unit vectors related to each direction. Unlike the linear variance that can take any positive value, the circular variance varies between zero (all unit vectors pointing in the same direction) and one (all unit vectors pointing in directions that cancel each other).

The probability density function used in DFN modeling to stochastically generate subseismic fracture orientations also requires a parameter called the Fisher coefficient that measures the dispersion in fracture directions (Mardia, 1972). The Fisher coefficient (K) is defined as $K = 1/V$ and ranges between one and infinity. A high Fisher coefficient is related to fractures organized primarily around one orientation, whereas a low value indicates fractures in many orientations.

Figure 4 shows photos of shale outcrops that correspond to areas of high and low Fisher coefficients. Even though the scales and perspectives are different and no fracture-density comparison can be made based on these photos, they do show that fracture dispersion can vary significantly among outcrops. To extract qualitative information about fracture dispersion, we drew straight lines over all fractures in each photo and plotted these segments centered in their middle point. The result of this qualitative interpretation shows that the Fisher coefficient increases from Eagle Ford to Whitby mudstone in the photos shown in Figure 4.

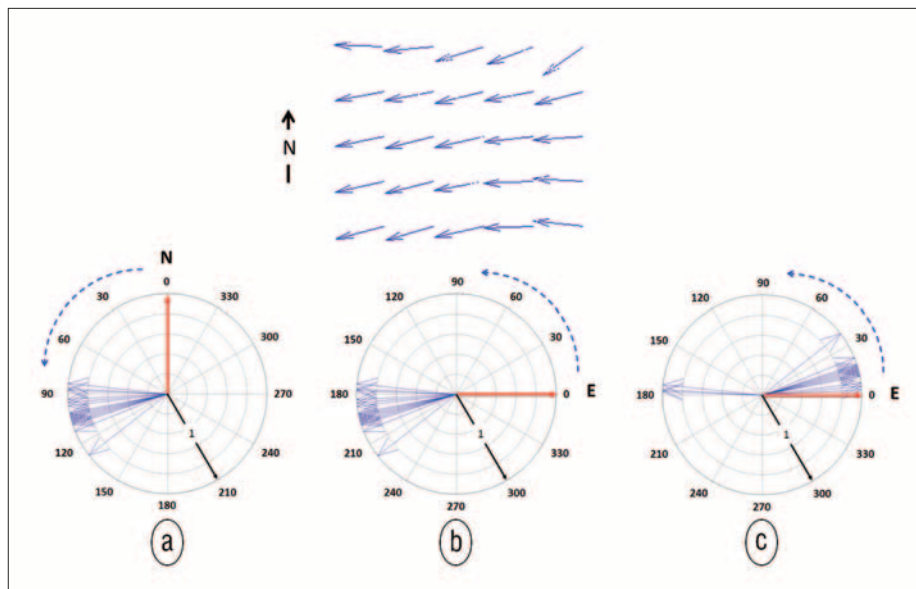


Figure 5. (top) Area with 25 predominantly east-west fractures. (bottom) Unit vectors that correspond to the 25 strike orientations. (a) All angles are referred to the north. In this case, the average magnitude of the sum of all unit vectors is $R/N = 0.9882$ (out of a maximum of one if all orientations were identical). (b) All angles are referred to the east. The sum of all unit vectors is the same as in part (a). (c) All angles are referred to the east, but 180° has been subtracted from orientations greater than 180° . Cases (b) and (c) represent identical fracture orientations. R/N decreases from 0.9882 in part (a) to 0.6863 in part (c) because in (c), directions along the east-west axis tend to cancel each other.

The estimation of a Fisher coefficient suitable for describing fracture orientations from the circular variance is not straightforward because the circular variance is designed to measure the spread in directions, not orientations. Because fracture planes have orientation but their dip-dependent direction is irrelevant to describe the relationship of their strike with respect to some reference axis in the horizontal plane, the Fisher coefficient estimated from the circular variance might not be totally adequate to describe variability in fracture orientations and might yield artificially low values in areas such as (i) (see Figures 2 and 3), where fractures show the same orientation but opposite directions that correspond to opposite dip directions. Eliminating the direction component by referring all angles to the range of 0° to 180° helps to alleviate this problem but does not solve it along whatever axis is chosen as a reference.

Let us examine this problem by analyzing in detail the estimation R/N in the simple example in Figure 5. Figure 5a shows all unit vectors in the upper part of the figure plotted from the same origin and referring the angles to the north. Because all angles fall in the range of 0° to 180° , there is no need to subtract 180° from the original angles, and the average magnitude of the sum of all unit vectors R/N is 0.9882 (out of a maximum of one if all unit vectors were identical).

Figure 5b shows the same unit vectors but now referring the angles to the east. When we choose this origin, we obtain some angles greater than 180° , and therefore, we need to refer some angles back to the interval of 0° to 180° . The result is shown in Figure 5c. Even though fracture orientations in Figure 5b and Figure 5c are the same, the average magnitude

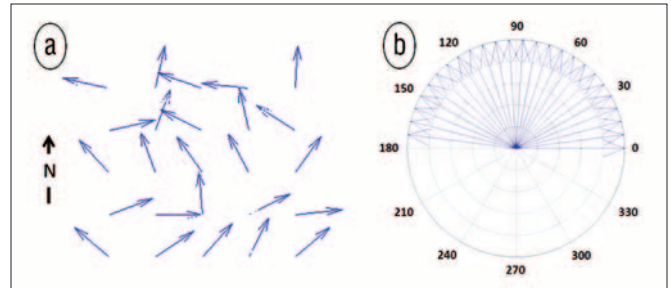


Figure 6. (a) Area with 25 random fracture orientations. (b) Random unit vectors referred to the interval zero to 180° . The average R/N of all 25 unit vectors in this case is 0.6358. For a continuum of random orientations, the average R/N is $2/\pi$ (≈ 0.6366).

R/N in Figure 5c is 0.6863, erroneously suggesting a larger dispersion than in Figure 5a, which represents identical fracture orientations. The reason for this apparent “error” is that orientations near the selected axis of reference for the angles might result in an artificially low sum of unit vectors if they point in nearly opposite directions.

In only two cases is the dispersion independent of the selection of the reference axis: (1) when all orientations are identical or (2) when dispersion is the highest and fractures are randomly oriented in the block of interest. All other intermediate cases that result in higher dispersion with respect to one axis will look lower with respect to another. As explained above, when all orientations are identical, we obtain $R/N = 1$. In the opposite extreme, when fractures are oriented randomly (as in Figure 6a), it is easy to show that $R/N \approx 0.6366$, which is the average of the sine function in the interval zero to π .

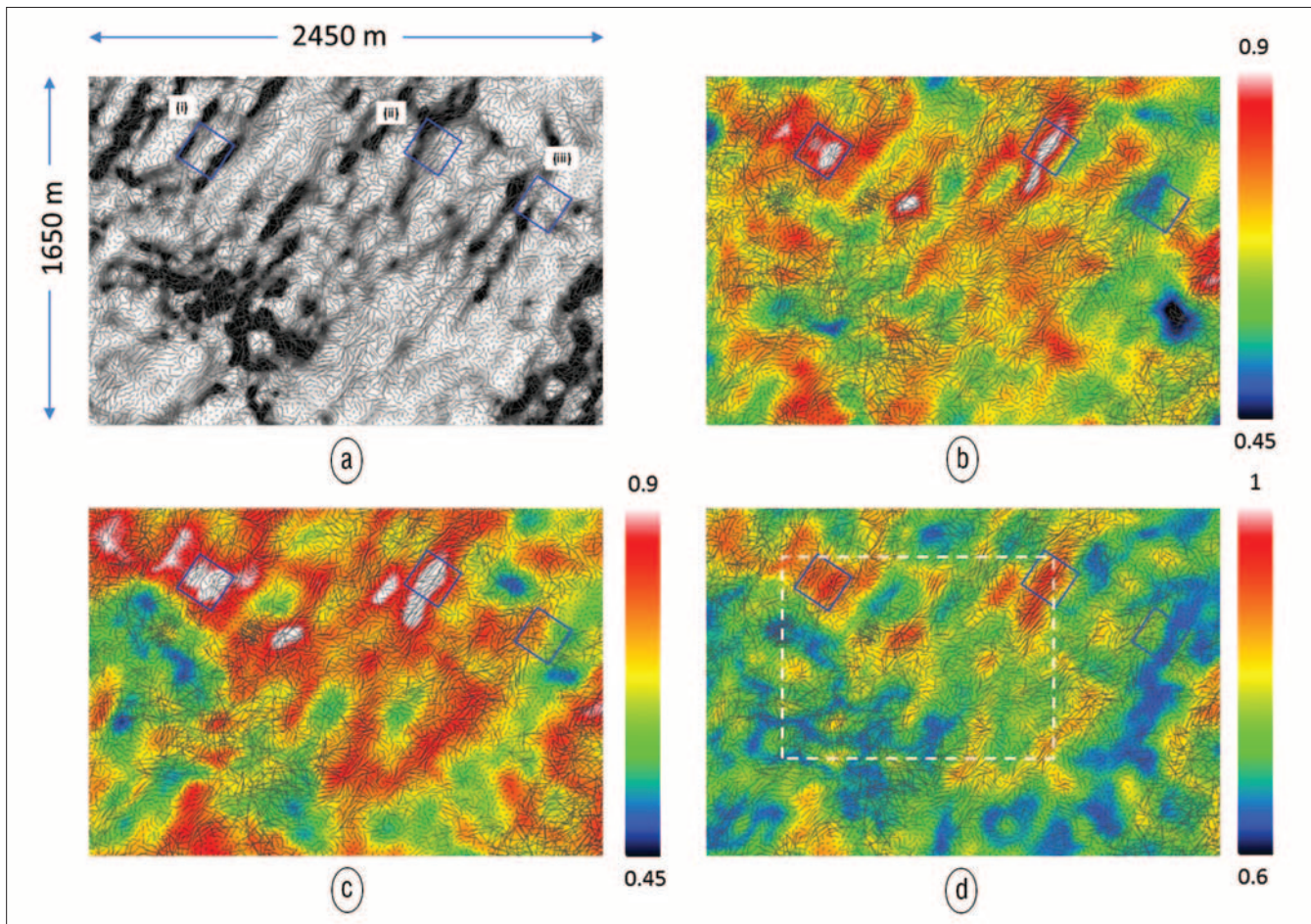


Figure 7. (a) Horizon slice of maximum curvature. (b) R/N estimated by referring all angles to the east. (c) R/N estimated by referring all angles to the north. (d) Maximum of R/N maps (b) and (c) which can be transformed into the Fisher coefficient for DFN modeling. See Figure 9d for the Fisher coefficient calculated from R/N inside the dashed white line in part (d). Original local fracture orientations are also shown in each horizon slice for reference.

The examples of Figure 5 and Figure 6 show extreme cases in orientation dispersion from all fractures clustered around a single angle to fractures spread uniformly across all angles. As we have discussed, if we estimate the dispersion by averaging the magnitude of the sum of unit vectors, the result will depend on the selection of the reference axis because fracture orientations near the reference may produce artificially low sums. However, these apparently low values that indicate high dispersion can be reestimated by using a reference axis that is orthogonal to the first axis. In other words, if we compute R/N in two orthogonal reference axes and select the highest value from the two results, we ensure that fracture dispersion will not be overestimated because of the proximity of the orientations to a particular reference axis.

To summarize, the steps needed to estimate orientation dispersion M at a point are:

- 1) Select the first of the two reference axes needed.
- 2) Generate dip-azimuth direction angles with respect to this axis.
- 3) Refer all direction angles to the orientations in the range of 0° to 180° .
- 4) Select a second reference axis orthogonal to the first one. Refer all angles to the new range of 0° to 180° .

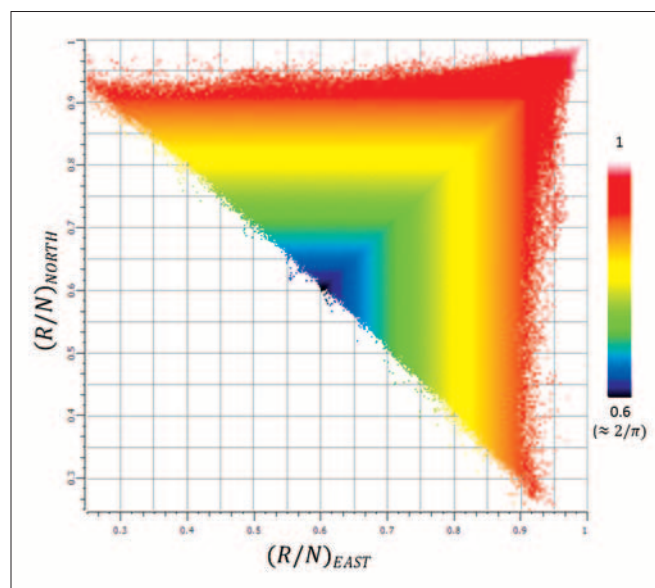


Figure 8. Crossplot of R/N estimated by referring all angles to the east and to the north. The color represents the maximum of the two axes. The minimum of R/N for each axis occurs in the upper vicinity of 0.6 which, as explained in Figure 6, corresponds to the case of randomly oriented fractures.

Downloaded 12/11/13 to 63.233.143.19. Redistribution subject to SEG license or copyright; see Terms of Use at http://library.seg.org/

- 5) Compute R/N for each set of orientation angles and extract the maximum M .

The estimate of dispersion M needs to be normalized between zero and one before it can be transformed into the Fisher coefficient required for DFN modeling. The minimum of M occurs when the orientations in the block of interest are completely random, which results, as we explained above, in $M = 2/\pi$ (a formal theoretical demonstration of this is beyond the scope of this article, but we will demonstrate it empirically in the field data example that follows). Based on this fact, it is easy to show that the Fisher coefficient K can be calculated by using the following expression:

$$K = \frac{1 - 2/\pi}{1 - M}. \quad (2)$$

Figure 7 shows the result of the estimation of R/N for different reference axes (Figure 7b and Figure 7c) and the maximum of the two (Figure 7d). Areas of low R/N indicate high dispersion of fracture orientation, and areas of high R/N indicate areas where fracture orientations do not change significantly. Figure 8 shows a crossplot of the values of R/N estimated by referring the angles to the east and to

the north. This crossplot is colored by the maximum of the two estimates. Notice how the minimum of R/N for each axis is approximately 0.6 which, as explained in Figure 6, corresponds to the case of randomly oriented fractures.

Application to DFN modeling

We built several discrete fracture models (DFM) using the methodology explained above, assuming fractures of constant aperture, height, and length. For this example, intensity (fracture area/unit volume, or P32, as commonly referred to in DFN modeling) is assumed to be proportional to the maximum curvature (Figure 9a). Figure 9b shows the dominant fracture orientations extracted from gradients computed from the maximum curvature (same as in Figure 2c). Figure 9c shows the Fisher coefficient derived from Figure 7d (inside dashed white line) using equation 2. Figure 9d shows the intersection of the stochastically modeled fractures with the horizon of interest. Notice how local orientations in this DFM are determined by both the dominant orientation and the local Fisher coefficient.

Application to flow simulation

To illustrate the effect of the Fisher coefficient on directional

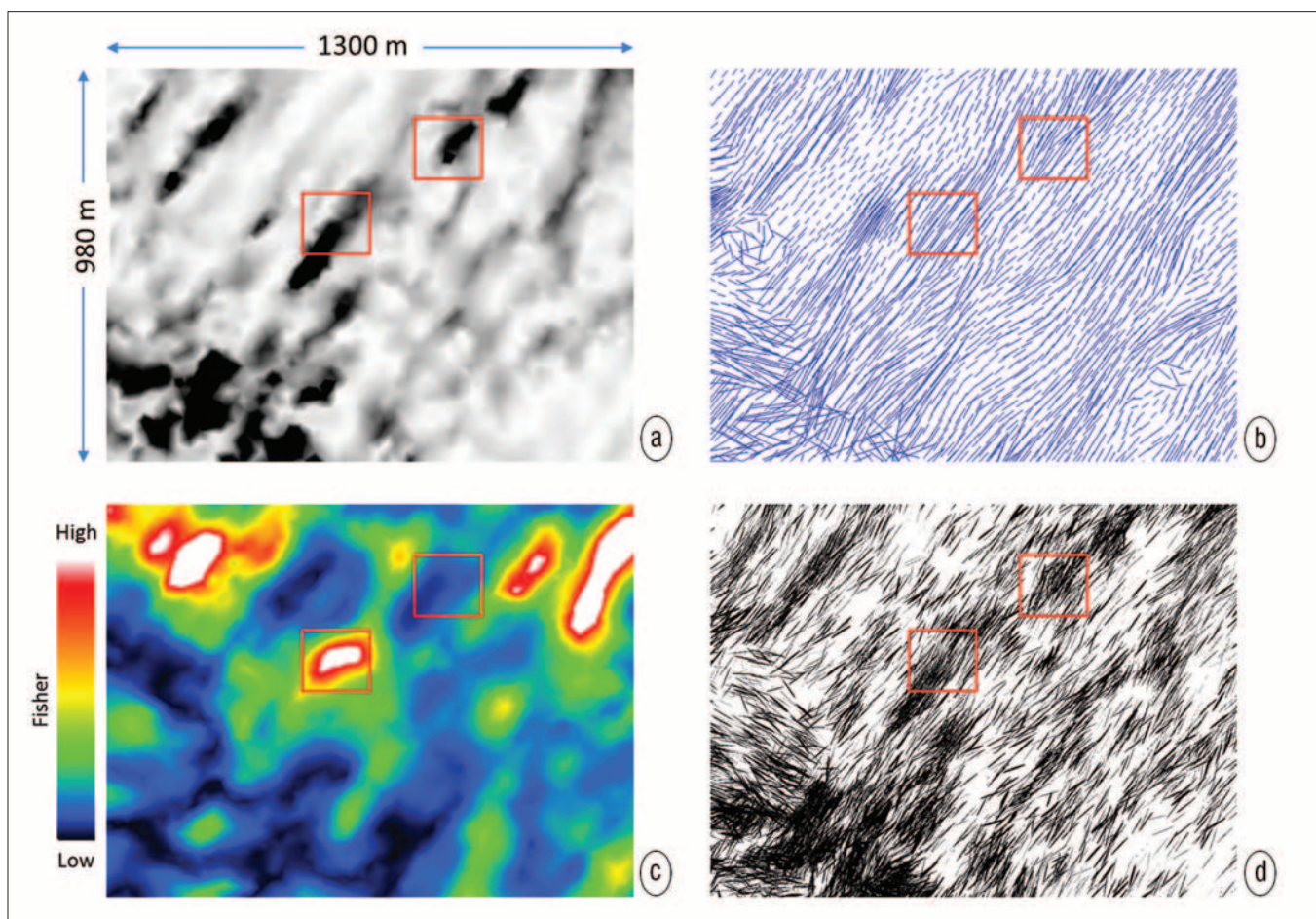


Figure 9. Seismic-constrained DFN modeling within the dashed rectangle shown in Figure 7d. (a) Original maximum curvature (assumed to be proportional to fracture intensity) along stratigraphic horizon. (b) Dominant orientation. (c) Fisher coefficient calculated from R/N inside dashed white line in Figure 7d. (d) DFN modeled fractures near the horizon of interest. Stochastically modeled fractures capture expected intensity, orientation, and local dispersion extracted from the seismic data. Areas inside red boxes have similar intensity and orientation but different Fisher coefficients.

permeability, we also defined two alternative DFMs with a large Fisher coefficient (1000) uniformly assigned throughout the model area resulting in strong directional permeability anisotropy around the dominant orientation and alternatively with a small Fisher coefficient (1) uniformly assigned throughout the model area, resulting in more isotropic permeability. There is still significant cell-to-cell permeability variation in both cases, as defined by variability in fracture intensity.

The average effective fracture permeability assumed for these DFMs is on the order of 0.5 mD (a typical value for Bakken Formation). The DFMs were then upscaled for dual-media flow-simulation models (Dershowitz et al., 2000; Oda, 1985) assuming a matrix permeability on the order of that seen in commercial unconventional reservoirs (1 mD) and were initialized with undersaturated oil on the order of 1-cp viscosity. Both models were then run with a horizontal well (Figure 10) producing at a fixed bottom-hole pressure of 500 psia. Initial pressure is 6750 psia. Along the horizontal wellbore, five times permeability enhancement (representing multistage hydraulic fracturing with 150-ft effective stimulated radius) is applied in the model. Figure 10a shows that reasonable unconventional well initial production (IP) rates have

been achieved through this near-wellbore permeability-enhancement approach.

Figure 10a also shows that the decline behavior for the simulations is consistent with that expected for unconventional reservoirs. However, both models show minimal rate differences, which demonstrates that decline behavior alone cannot distinguish the nature of the pressure depletion in the reservoir. Figure 10b and Figure 10c show the pressure for each model (high and low Fisher coefficient, respectively) after 100 days of simulation. The absolute pressures look similar except for small differences in zones of large fracture intensity.

Figure 10d compares the pressure difference for the two models. Blue colors represent the case in which the large uniform Fisher coefficient results in lower pressure than the small Fisher coefficient. Red represents the reverse situation. The trends in blue shading show that when open fracturing is intense and highly directional (large permeability anisotropy), the pressure depletion is more localized to the areas of high fracture intensity. In the case with a low Fisher coefficient, the pressure wave will move more slowly away from the well in these highly fractured areas, resulting in more uniform depletion all along the well, as shown by the red coloring, even in lower-intensity areas.

The impact of stress on the permeability on individual fractures has not been incorporated in this simulation study,

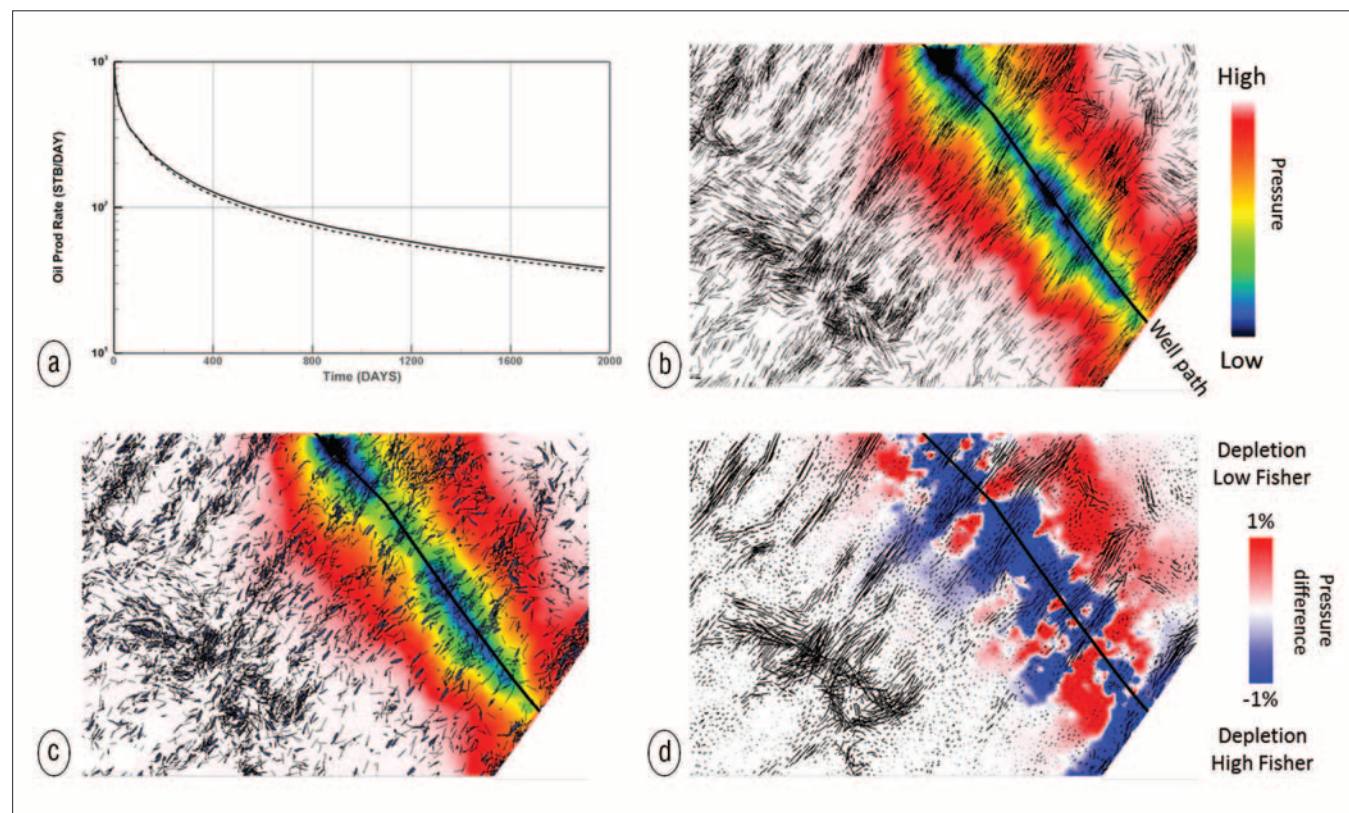


Figure 10. (a) Decline behavior of two models with high (1000, dashed line) and low (1, continuous line) Fisher coefficient. (b) Pressure in model with uniform Fisher coefficient of 1000 after 100 days of simulation. Black segments indicate DFN-modeled fractures near the horizon of interest. (c) Pressure in model with uniform Fisher coefficient of 1 after 100 days of simulation. DFN-modeled fractures are also shown. Notice how both pressure fields are similar despite the large difference in Fisher coefficient. (d) Pressure difference. Black segments indicate dominant orientation from seismic whose length is proportional to the local curvature. Blue colors represent the case in which the large uniform Fisher coefficient results in lower pressure than the small Fisher coefficient. Red represents the reverse situation. The trends in blue shading show that when open fracturing is intense and highly anisotropic, pressure depletion is more localized to the areas of high fracture intensity.

and it is expected that favorably oriented fractures are more likely to be naturally open or to open under shear during hydraulic-fracture operations. Calibration of the seismic interpretation to FMI, microseismic, hydraulic-fracturing treatment pressures, well tests, offset well interference, and production decline, all within the confines of geo-mechanical constraints, is required to better characterize the depletion behavior and to optimize hydraulic-fracture treatments and well spacing in naturally fractured unconventional reservoirs

Discussion and conclusions

We have presented a methodology to estimate dominant fracture orientation and orientation dispersion from seismic data and to use this information to constrain DFN and flow-simulation models. The estimation of dispersion (Fisher coefficient) is based on the maximum circular variance extracted from two orthogonal axes for the origin of angles. By estimating the variance for two axes and extracting the maximum, we circumvent the intrinsic limitation of the circular variance that is designed to measure spread in directions, not orientations. Three-dimensional dispersion estimates from seismic data show lateral variability that is not possible to quantify by using 1D well data alone.

We also show flow-simulation examples in models built using different dispersion conditions to assess the effect of dispersion in permeability anisotropy. These flow-simulation models are built with parameters typical of those in an unconventional reservoir. The simulations show that fracture dispersion is expected to have significant implications on fluid-flow behavior because of the impact on natural fracture permeability behavior prior to and subsequent to hydraulic-fracturing treatments.

For the cases illustrated here, high-intensity fractured areas (fracture swarms) with large Fisher coefficients will result in significant pressure-depletion pathways extending away from wells and nonuniform pressure depletion along the well path. Although not illustrated here, nonuniform flow behavior will be even more severe during injection processes (e.g., miscible gas, surfactant, or water).

As mentioned in the introduction, the estimation of fracture orientation from AVOZ analysis typically assumes a single set of vertical fractures. In terms of velocity anisotropy, this situation can be described by a horizontal transversely isotropic model (HTI) which corresponds to the case of high Fisher coefficient. A low Fisher coefficient corresponds to fractures with many orientations which, from the wave-propagation point of view, behave like an isotropic model. Velocity anisotropy models for situations that require symmetries more complex than HTI (from orthorhombic to triclinic) will result in intermediate Fisher coefficients, but the actual correspondence among them (if any) requires further research.

More research is also needed to understand the effect of orientation dispersion in hydraulic fracturing as well as other issues such as fracturing scale, calibration with dispersion from log data, and number of fracture families. **TLE**

References

- Chopra, S., K. J. Marfurt, and H. T. Mai, 2009, Using automatically generated 3D rose diagrams for correlation of seismic fracture lineaments with similar lineaments from attributes and well log data: *First Break*, **27**, no. 10, 37–42, <http://dx.doi.org/10.3997/1365-2397.2009016>.
- Dershowitz, W., P. LaPointe, T. Eiben, and L. Wei, 2000, Integration of discrete fracture network methods with conventional simulator approaches: *SPE Reservoir Evaluation & Engineering*, **3**, no. 2, 165–170, <http://dx.doi.org/10.2118/62498-PA>.
- Fisher, N. I., 1995, *Statistical analysis of circular data*: Cambridge University Press.
- Mardia, K. V., 1972, *Statistics of directional data*: Academic Press.
- Oda, M., 1985, Permeability tensor for discontinuous rock masses: *Géotechnique*, **35**, no. 4, 483–495, <http://dx.doi.org/10.1680/geot.1985.35.4.483>.
- Will, R., R. A. Archer, and W. S. Dershowitz, 2005, Integration of seismic anisotropy and reservoir-performance data for characterization of naturally fractured reservoirs using discrete-feature-network models: *SPE Reservoir Evaluation & Engineering*, **8**, no. 2, 132–142, <http://dx.doi.org/10.2118/84412-PA>.

Acknowledgments: Thanks to Ezequiel Gonzalez for suggestions that added clarity to the article. Thanks also to Jonny Imber, Gary Lash, and Aiko Heiwa for permission to use their photos.

Corresponding author: michelena@ireservoir.com